Instability of the halocline at the North Pole

Christian Puntini

Faculty of Mathematics, University of Vienna, Oskar-Morgenstern-Platz 1, 1090, Vienna, Austria. ABSTRACT: In this paper we address the issue of stability for the near-inertial Pollard waves, as a model for the halocline in the region of the Arctic Ocean centered around the North Pole, derived in Puntini (2025a). Adopting the short-wavelength instability approach, the stability of such flows reduces to study the stability of a system of ODEs along fluid trajectories, leading to the result that, when the steepness of the near-inertial Pollard waves exceeds a specific threshold, those waves are linearly unstable. The explicit dispersion relation of the model allows to easily compute such threshold, knowing the physical properties of the water column.

1. Introduction

Exact solutions, albeit being quite rare, are fundamental tools in the study of (geophysical) fluid flows. Even if typically they describe ideal conditions that may not correspond with the actual complexities of the observed fluid dynamics, they can provide the basis for more directly relevant analyses: small perturbations can be superimposed on the existing exact solution to describe more complex flows. The main cause of the lack of explicit solutions in geophysical fluid dynamics is the nonlinear character of the governing equations, making direct computations very complicated. The first explicit exact solution of the (nonlinear) governing equation was found by Gerstner, for a homogeneous fluid, in 1809 (Gerstner 1809). It was later rediscovered by Froude (1862), Rankine (1863) and Reech (1869), and extended to heterogeneous fluid by Dubreil-Jacotin (1932). Gerstner's wave solution describes two-dimensional gravity water waves, starting from the assumption that fluid particles move in a circular motion with radius diminishing with the distance from the surface

$$\begin{cases} x = a - \frac{1}{k} e^{kb} \sin\left(ka - \sqrt{gk}\,t\right), \\ z = b + \frac{1}{k} e^{kb} \cos\left(ka - \sqrt{gk}\,t\right), \end{cases}$$
 (1)

where x and z are the horizontal and vertical coordinates at time t of the particle labeled by the real parameters a and b, with $b \le b_0 < 0$. See (Henry 2008; Constantin 2011; Abrashkin and Pelinovsky 2022; Stuhlmeier 2015) for a modern review of Gerstner's solution.

One essential feature of the aforementioned solution is that it is found in the Lagrangian formalism. Lagrangian solutions have the advantage that the fluid kinematics can easily described explicitly (see (Bennett 2006)), as in the Lagrangian framework one specifies the motion of each fluid particle, whereas in the Eulerian framework the fluid motion is described by the determination of the fluid velocity at a fixed point in space.

The Lagrangian formalism has resulted to be particularly useful to find exact solutions to many models in the oceanography context. Pollard (1970) generalized Gerstner's trochoidal solution to account for Earth's rotation, and, more recently, Gerstner-like solutions were used to describe equatorial waves (Constantin 2012a,b, 2013, 2014; Henry 2016), wave-current interactions (Constantin and Monismith 2017; McCarney 2023, 2024) and edge waves (Mollo-Christensen 1979; Constantin 2001; Ionescu-Kruse 2015a; Weber 2012; Miao et al. 2022; Stuhlmeier 2014). See

also (Stuhlmeier 2013) for Gerstner waves in the case of a still-water surface and (Ionescu-Kruse 2015b) for Pollard waves in equatorial regions.

Once an exact solution is given, a natural question that arises is its stability. Broadly speaking, a flow is stable when small perturbations do not alter the main characteristics of the motion, whereas instability occurs when the effects of some disturbances grow with time (see Constantin and Germain (2013); Drazin and Reid (2004)).

The aim of this paper is to present a stability analysis of a three-dimensional geophysical flow derived in (Puntini 2025a) to describe the halocline of the region of the Arctic Ocean centered around the North Pole via a 3-layer model. We adopt the short-wavelength instability approach (developed by Bayly (1987), Friedlander and Vishik (1991) and Lifschitz and Hameiri (1991)), which is particularly suited for flows described in the Lagrangian framework, that has been used to prove instability of many models in oceanography (see (Constantin and Germain 2013; Chu et al. 2019b,a; Ionescu-Kruse 2015c, 2016a; Miao et al. 2022; Ionescu-Kruse 2016b, 2017)).

The paper is structured as follows: Section 2 provides an overview of the fundamental characteristics of the Arctic halocline and the mathematical model employed, before establishing the governing equations that describe the flow dynamics of interest, and reviewing the nonlinear solution developed in (Puntini 2025a) that describes the Arctic halocline via near-inertial Pollard waves. We remark that we are focusing only on the central part of the Arctic Ocean, around the North Pole. Section 3 contains the main result of this work: the instability of the near-inertial Pollard waves describing the halocline. Using the short-wavelength instability approach (developed in (Ionescu-Kruse 2016b) for Pollard waves), stability is studied by analyzing a system of ODEs along the fluid particle paths, and a criterion for instability is established: if the wave steepness exceeds a certain threshold, the waves become unstable. The explicit dispersion relation of the solution allows for straightforward computation of the numerical values of this threshold, given the physical properties of the water column. Finally, we conclude with a discussion of the results in Section 4.

2. Description of the flow and governing equations

The Arctic halocline represents a region of pronounced stratification that prevents -in the central region of the Arctic Ocean- sea ice from thermally interacting with the warmer, more saline

Atlantic Water located in the deeper portions of the water column. The Arctic Ocean exhibits a distinctive vertical structure comprising several distinct layers. The surface mixed layer consists of cold, fresh water extending from 5 to 100 meters in depth. Below this lies the halocline, which extends to depths of 40-200 meters, underlain by a layer of relatively warm, saline Atlantic Water (Metzner and Salzmann 2023; Peralta-Ferriz and Woodgate 2015). The deepest stratum consists of Arctic Deep Water. As this deepest layer is not relevant to our model, we focus exclusively on the uppermost three layers. Moreover, it is worth remarking that variations in the structure of the Arctic Ocean, especially in its central part, have been established as indicators of the global warming (see e.g. Morison et al. (2018); Polyakov et al. (2018)).

These layer boundaries undergo seasonal variations in response to temperature fluctuations and sea ice dynamics. For example, winter conditions, characterised by lower temperatures and expanded ice coverage, force the upper boundary of the halocline to greater depths within the water column. Conversely, summer warming and ice retreat cause the layer to migrate toward the surface (Peralta-Ferriz and Woodgate 2015).

Physical processes within the mixed layer, primarily ice motion driven by wind forcing and the Transpolar Drift Current (TDC), generate significant flow at the base of the mixed layer. The TDC represents the dominant Arctic Ocean current that transports surface waters and sea ice from the Laptev Sea and East Siberian Sea toward Fram Strait at velocities of approximately 0.07ms^{-1} in the vicinity of the North Pole. These processes collectively induce currents with magnitudes of approximately 0.1ms^{-1} at the lower boundary of the mixed layer (see Guthrie et al. (2013)).

Although the halocline exhibits regional variations—including the cold halocline layer in the Eurasian Basin, the Pacific Halocline Waters in the Amerasian Basin, and the lower halocline water (Metzner and Salzmann 2023)—the simplified model employed herein assumes constant densities within each layer under consideration, as we are considering a relatively small region of the Arctic Ocean centered around the North Pole. This assumption is also justified by the minimal density variations observed within individual strata (Polyakov et al. 2018). Our model incorporates three constant densities: ρ_0 , ρ_1 and ρ_2 , where $\rho_0 < \rho_1 < \rho_2$. Here, ρ_0 represents the fresh, cold water of the surface mixed layer above the halocline, ρ_1 denotes the density of halocline water, and ρ_2 corresponds to the density of the saltier, warmer Atlantic Water (AW) below the halocline (see Fig. 1).

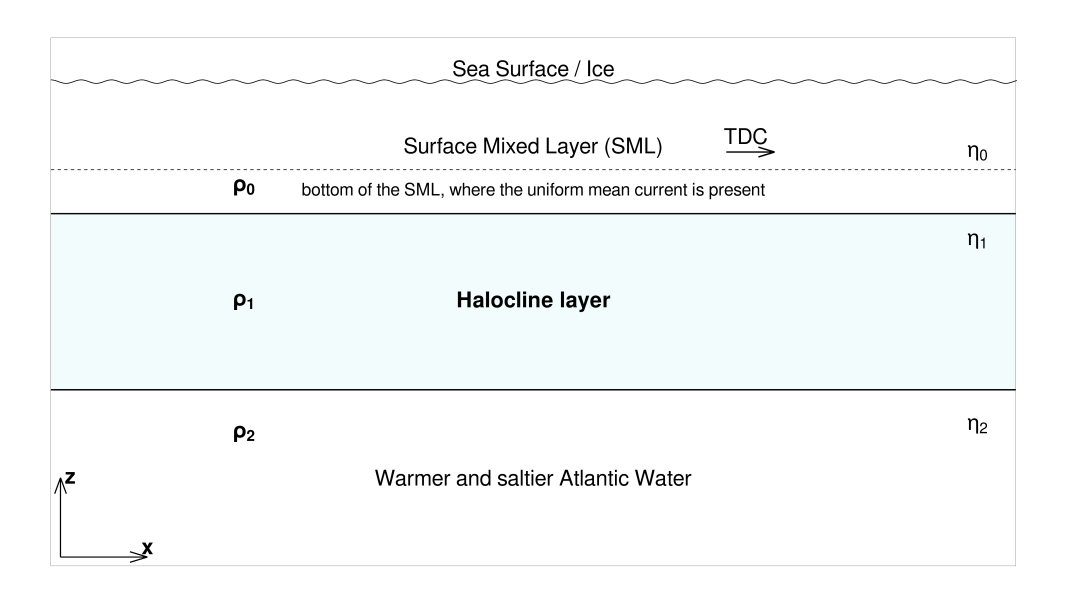


Fig. 1. A depiction of the model we are considering, consisting of 3 layer: the surface mixed layer (of density ρ_0) at which bottom the mean surface current is present, the halocline layer (of density ρ_1) and the bottom layer consisting of Atlantic Water (AW) with density ρ_3 .

With increasing depth, the influence of surface turbulence diminishes progressively, particularly in the presence of ice cover (which is a characteristic of the central part of the Arctic Ocean, subject of our investigation). Consequently, we postulate the existence of a potentially thin layer immediately above the lower boundary of the Surface Mixed Layer (SML), denoted as η_1 , wherein the fluid exhibits unidirectional flow aligned with the Transpolar Drift Current (TDC) at a mean velocity of approximately $0.1 \,\mathrm{ms}^{-1}$. The upper boundary of this layer is designated as η_0 ; however, as will become apparent from our subsequent analysis, the specific functional form of η_0 does not influence our theoretical framework. Furthermore, we adopt the assumption that the layer beneath the halocline remains essentially motionless, with its lower boundary denoted as η_2 , representing the bottom interface of the halocline. See Fig. 1.

Having established our model framework for the region of the Arctic Ocean around the North Pole, we now proceed to briefly set forth the governing equations. Away from the boundary layers, friction and viscous effects are negligible, allowing the fluid to be treated as ideal (Maslowe 1986; Constantin and Johnson 2019). Consequently, the momentum equations governing the fluid motion

take the form of the Euler equations, and, as the region of the flow we are considering is relatively small, we can adopt an f-plane approximation, with the axis \mathbf{e}_x aligned with the Transpolar Drift Current and the axis \mathbf{e}_y perpendicular to it (see Fig. 2). The \mathbf{e}_z -axis, as usual, points upward. It is worth noting that such f-plane approximation is not built starting from the governing equations in the classical spherical coordinates, but in the "rotated" spherical coordinate system developed in (Constantin and Johnson 2023) suitable for the North Pole (where the classical spherical coordinates fail). We refer to (Puntini 2025a) for a more in-detail exposition of the governing equations (see also (Puntini 2025b) for an in-depth derivation of the governing equation in this new rotated coordinate system).

Therefore, the Euler equations in the f-plane approximation read as

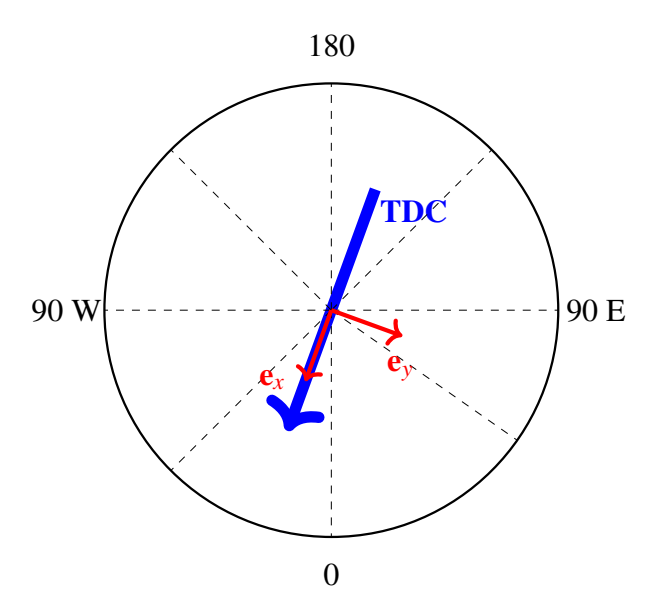


Fig. 2. Depiction of the basis at the North Pole, with \mathbf{e}_x aligned with the Transpolar Drift Current and \mathbf{e}_y perpendicular to it. The \mathbf{e}_z -axis, as usual, points upward.

$$\begin{cases} U_{t} + UU_{x} + VU_{y} + WU_{z} - fV = -\frac{1}{\rho}P_{x}, \\ V_{t} + UV_{x} + VV_{y} + WV_{z} + fU = -\frac{1}{\rho}P_{y}, \\ W_{t} + UW_{x} + VW_{y} + WW_{z} + g = -\frac{1}{\rho}P_{z}, \end{cases}$$
(2)

where $f = 2\Omega \approx 1.5 \cdot 10^{-4} \,\mathrm{s}^{-1}$ and $(U, V, W) =: \mathbf{U}$ are the velocity component associated to the basis $(\mathbf{e}_x, \mathbf{e}_y, \mathbf{e}_z)$, and pedices x, y, z, t indicate partial derivatives. The density ρ in (2) will be set equal to ρ_0 , ρ_1 or ρ_2 depending on the layer of the fluid we are considering.

Moreover, the seawater is treated as incompressible, as a change of about 500 kPa in pressure leads to only a 0.025% change in the water density (see (Maslowe 1986)), giving that the incompressibility condition

$$U_x + V_y + W_z = 0, (3)$$

must hold, as well as the mass conservations

$$\rho_t + U\rho_x + V\rho_y + W\rho_z = 0. \tag{4}$$

As we are considering constant densities, (4) is always satisfied.

In addition to the governing equations (2) and (3) we require the solution to satisfy the dynamic boundary condition (i.e. the pressure must be continuous across the surfaces η_1 and η_2), and the kinematic boundary condition

$$W = \eta_{i,t} + U\eta_{i,x} + V\eta_{i,y}$$
 on $z = \eta_i$, $i = 1, 2$, (5)

preventing the mixing of fluid particles between different layers (see (Constantin 2011)). Due to their different character, we will describe the flow in each layer separately.

a. The deep motionless layer beneath the halocline

In the region $z < \eta_2(x - ct, y)$ the water is in hydrostatic state u = v = w = 0, hence (2) reads as

$$\begin{cases} \frac{\partial P}{\partial x} = 0, \\ \frac{\partial P}{\partial y} = 0, \\ \frac{\partial P}{\partial z} = -\rho_2 g, \end{cases}$$
 (6)

giving, for the pressure,

$$P(x, y, z) = P_2 - \rho_2 g z, \tag{7}$$

with $P_2 \in \mathbb{R}$. Being hydrostatic, the flow is irrotational and satisfies the continuity equation (3).

b. The halocline layer $\mathcal{H}(t)$

We denote by $\mathcal{H}(t)$ the halocline layer: $\eta_2(x-ct,y) \le z \le \eta_1(x-ct,y)$. Differently from the previous layer, we seek an explicit solution of (2), (3) and (5), fulfilling also the dynamic and kinematic boundary conditions, in the Lagrangian formalism: at time t we specify the position $\mathbf{X} = (x, y, z)$ of the fluid particles in terms of the labeling variables (q, r, s) by

$$\begin{cases} x = q - be^{-ms} \sin(k(q - ct)), \\ y = r - de^{-ms} \cos(k(q - ct)), \\ z = -d_0 + s - ae^{-ms} \cos(k(q - ct)). \end{cases}$$
(8)

The constant $k = \frac{2\pi}{L} > 0$ is the wave number corresponding to the wavelength L, and we assume m > 0 and a > 0, while the labeling variables are chosen so that

$$(q,r,s) \in \mathbb{R} \times [-\mathcal{R},\mathcal{R}] \times [s_{-}(r),s_{+}(r)], \tag{9}$$

where $s = s_-(r) \ge s^* > 0$ represents η_2 , $s = s_+(r) > s_-(r)$ represents η_1 and $\Re \approx 15$ km is the Rossby radius of deformation (see (Gill 1982)), and $d_0 - s_-$ is the mean depth of the halocline base. Moreover, the following relation on the parameters must be satisfied (see (Puntini 2025a) for more details)

$$b = \frac{ma}{k}, \qquad d = -\frac{fma}{k^2 c}, \qquad m^2 = \frac{k^4 c^2}{k^2 c^2 - f^2}, \qquad a^2 + d^2 = b^2.$$
 (10)

The particle paths are depicted in Fig 3.

The Jacobian of the map (8) relating the particle positions with the Lagrangian labeling variables is given by (using the relations in (10))

$$\left(\frac{\partial(x,y,z)}{\partial(q,r,s)}\right) := \begin{pmatrix} x_q & y_q & z_q \\ x_r & y_r & z_r \\ x_s & y_s & z_s \end{pmatrix} = \begin{pmatrix} 1 - ma e^{-ms} \cos\Theta & -f \frac{ma}{kc} e^{-ms} \sin\Theta & kae^{-ms} \sin\Theta \\ 0 & 1 & 0 \\ \frac{m^2 a}{k} e^{-ms} \sin\Theta & -f \frac{m^2 a}{k^2 c} e^{-ms} \cos\Theta & 1 + mae^{-ms} \cos\Theta \end{pmatrix}, (11)$$

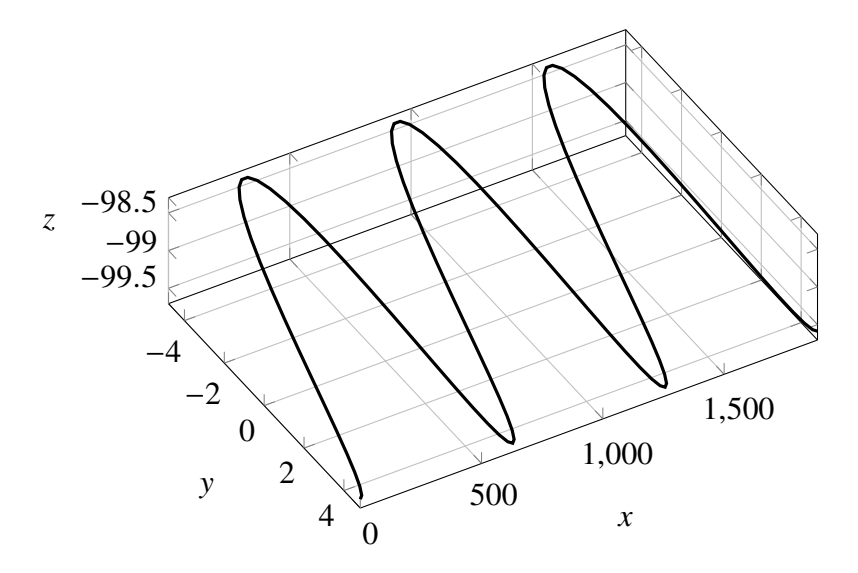


Fig. 3. Trochoid described in (8), with labeling variables $q \in [0,600\pi]$, r = 0, s = 1 and parameters a = 1, $d_0 = 100$ and b, d, m given by (10) (the dispersion relation is given by (35)). The 2-dimensional surface is obtained by collecting all the translation of this curve in the horizontal y-direction.

where we denoted

$$\Theta = k(q - ct), \tag{12}$$

and its determinant is equal to

$$\Delta = 1 - m^2 a^2 e^{-2ms} > 0. \tag{13}$$

Therefore, as the determinant in (13) is non-zero and time-independent, the flow is incompressible (see (Constantin 2011; McCarney 2024)) and (3) is satisfied. The velocity and acceleration of a particle can be computed using (8), giving respectively

$$\begin{cases} U = \frac{Dx}{Dt} = kcb e^{-ms} \cos\Theta, \\ V = \frac{Dy}{Dt} = -kcd e^{-ms} \sin\Theta, \\ W = \frac{Dz}{Dt} = -kca e^{-ms} \sin\Theta, \end{cases} \text{ and } \begin{cases} \frac{DU}{Dt} = k^2c^2b e^{-ms} \sin\Theta, \\ \frac{DV}{Dt} = k^2c^2d e^{-ms} \cos\Theta, \\ \frac{DW}{Dt} = k^2c^2a e^{-ms} \cos\Theta. \end{cases}$$
(14)

From the governing equations (2), making use of (14) we obtain the following expression for the pressure in the halocline layer $\mathcal{H}(t)$:

$$P(q - ct, r, s) = P_1 - \rho_1 gs + \frac{\rho_1}{2} (b^2 k^2 c^2 + fb dk c) e^{-2ms} + \rho_1 (bk c^2 + df c + ga) e^{-ms} \cos \Theta.$$
(15)

c. The layer $\mathcal{M}(t)$ above the halocline

The layer above the halocline, denoted by $\mathcal{M}(t)$, is bounded below by the halocline upper surface η_1 and above by η_0 . Its internal wave motion is due to the oscillations of the halocline, and - as physical measurements highlights the presence of a mean current of about $0.1\,\mathrm{ms}^{-1}$ in the direction of the Transpolar Drift Current (Guthrie et al. 2013) - we include such feature by assuming a uniform horizontal current in the *x*-direction (in our coordinate system aligned with the TDC), denoted by \mathbf{c}_0 .

As for the previous layer, we provide a description of the fluid flow in the Lagrangian framework. The position $\mathbf{X} = (x, y, z)$ of the fluid particles at time t in terms of the labeling variables (q, r, s) is given by

$$\begin{cases} x = q - be^{-ms} \sin(k(q - ct)) - c_0 t, \\ y = r - de^{-ms} \cos(k(q - ct)), \\ z = -d_0 + s - ae^{-ms} \cos(k(q - ct)). \end{cases}$$
(16)

Again, the constant $k = \frac{2\pi}{L} > 0$ is the wave number corresponding to the wavelength L, m > 0 and a > 0, while the labeling variables are now chosen so that

$$(q,r,s) \in \mathbb{R} \times [-\mathcal{R},\mathcal{R}] \times [s_+(r),s_0(r)], \tag{17}$$

where $s = s_+(r)$ represents η_1 and the parameter $\mathcal{R} \approx 15 \,\mathrm{km}$ is the Rossby radius, as before, and the relations (10) still apply; moreover $s = s_0(r)$ represents the upper surface η_0 of the layer $\mathcal{M}(t)$.

The Jacobian of the map (16) is the same as the one of (8), that is

$$\left(\frac{\partial(x,y,z)}{\partial(q,r,s)}\right) = \begin{pmatrix}
1 - ma e^{-ms} \cos\Theta & -f \frac{ma}{kc} e^{-ms} \sin\Theta & kae^{-ms} \sin\Theta \\
0 & 1 & 0 \\
\frac{m^2a}{k} e^{-ms} \sin\Theta & -f \frac{m^2a}{k^2c} e^{-ms} \cos\Theta & 1 + mae^{-ms} \cos\Theta
\end{pmatrix},$$
(18)

with determinant

$$\Delta = 1 - m^2 a^2 e^{-2ms} > 0, (19)$$

providing, as before, a proof that the flow described by (16) satisfies the incompressibility condition (3). The velocity and acceleration of a particle in this layer are given by

$$\begin{cases} U = \frac{Dx}{Dt} = kcb e^{-ms} \cos\Theta - c_0, \\ V = \frac{Dy}{Dt} = -kcd e^{-ms} \sin\Theta, \\ W = \frac{Dz}{Dt} = -kca e^{-ms} \sin\Theta, \end{cases} \quad \text{and} \quad \begin{cases} \frac{DU}{Dt} = k^2 c^2 b e^{-ms} \sin\Theta, \\ \frac{DV}{Dt} = k^2 c^2 d e^{-ms} \cos\Theta, \\ \frac{DW}{Dt} = k^2 c^2 a e^{-ms} \cos\Theta. \end{cases}$$
(20)

Analogously, to the previous layer, inserting (20) into the governing equations (2) and integrating allows to obtain the following expression for the pressure (recalling that we are now in the layer with density ρ_0 , and we made use of (10))

$$P(q - ct, r, s) = P_0 - \rho_0 g s + \rho_0 f c_0 r + \frac{\rho_0}{2} (b^2 k^2 c^2 + f b d k c) e^{-2ms} + \rho_0 (b k c^2 + d f c + g a - d f c_0) e^{-ms} \cos \Theta$$
(21)

The dispersion relation and the expression for the wavenumber $k = \frac{2\pi}{L}$, as well as the existence of η_2 and η_1 , will be provided by imposing the dynamic boundary condition across the surfaces η_1 and η_2 .

d. The upper and lower surfaces of the halocline, and the dispersion relation

For every $r \in [-\mathcal{R}, \mathcal{R}]$, the upper surface of the halocline η_1 is described by $s = s_+(r)$, and the continuity of the pressure is imposed by equaling (15) and (21) at $s = s_+(r)$, giving

$$\begin{cases} P_0 - P_1 = \left(\frac{\rho_1 - \rho_0}{2}\right) k^2 c^2 a^2 e^{-2ms_+} - (\rho_1 - \rho_0) g s_+ - \rho_0 f c_0 r, \\ \rho_1 \left(bkc^2 + df c + g a\right) = \rho_0 \left(bkc^2 + df c + g a - df c_0\right). \end{cases}$$
(22)

The upper surface of the halocline, η_1 , is determined by setting $s = s_+(r)$ at a fixed value of $r \in [-\mathcal{R}, \mathcal{R}]$, where $s_+(r)$ is the unique solution of

$$P_0 - P_1 = \left(\frac{\rho_1 - \rho_0}{2}\right) k^2 c^2 a^2 e^{-2ms_+} - (\rho_1 - \rho_0) g s_+ - \rho_0 f c_0 r.$$
 (23)

Analogously, for every $r \in [-\mathcal{R}, \mathcal{R}]$, the lower surface of the halocline η_2 (also called halocline base) is described by $s = s_-(r)$. Setting the expression for the pressure in (15) equal to the one in (7) at $s = s_-(r)$, provides the fulfillment of the dynamic boundary condition at η_2 , if the following are satisfied

$$\begin{cases} P_{2} - P_{1} = \frac{1}{2} \rho_{1} b k \mathbf{c} (b k \mathbf{c} + d f) e^{-2ms_{-}} + (\rho_{2} - \rho_{1}) g s_{-} - \rho_{2} g d_{0}, \\ b k \mathbf{c}^{2} = \frac{\rho_{2}}{\rho_{1}} g a - g a - d f \mathbf{c}. \end{cases}$$
(24)

The halocline base η_2 is determined by setting $s = s_-(r)$ at a fixed value of $r \in [-\mathcal{R}, \mathcal{R}]$, where $s_-(r)$ is the unique solution of

$$P_2 - P_1 = \frac{1}{2}\rho_1 bk c(bkc + df)e^{-2ms} + (\rho_2 - \rho_1)gs - \rho_2 gd_0.$$
 (25)

The existence and uniqueness of $s_+(r)$ and $s_-(r)$ via the implicit function theorem are covered in (Puntini 2025a). See Fig. 4 for a depiction of the flow pattern.

Evaluating (23) at $s = s_+(r)$ and differentiating with respect to r gives

$$s'_{+}(r) = -\frac{\rho_0}{(\rho_1 - \rho_0)} \frac{f c_0}{(mk^2 c^2 a^2 e^{-2ms_+(r)} + g)}.$$
 (26)

Since the denominator in (26) is positive, the sign of c_0 determines whether the upper surface of the halocline rise or fall with respect to r. Observations show that the upper surface of the halocline

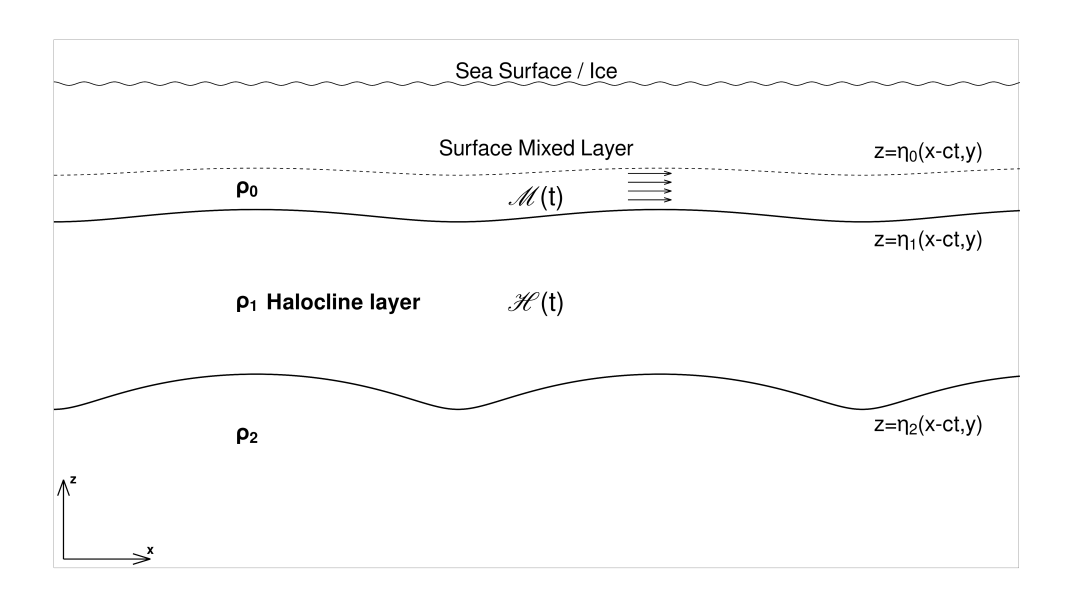


Fig. 4. Schematic depiction of the flow pattern, at a fixed coordinate y.

becomes shallower as r increases in the Eurasian Basin and deeper as r decreases in the Amerasian Basin (see (Polyakov et al. 2018)). This behavior requires $s'_+(r) > 0$ in (26), which implies $c_0 < 0$. The same conclusion can be obtained by observing the mean properties of the flow. We anticipate that the mean Lagrangian velocity in the x-direction is equal to $-c_0$ (see equation (46)), therefore, in order to have a mean flow in the direction of the TDC (which is an assumption of our model) we need to have $-c_0 > 0$, i.e. $c_0 < 0$.

Observe that, from second equation in (22), which, making use of (10), can be rewritten as

$$(\rho_1 - \rho_0) \left(g + |\mathbf{c}| \sqrt{k^2 \mathbf{c}^2 - f^2} \right) = \rho_0 \frac{f^2 |\mathbf{c}|}{\sqrt{k^2 \mathbf{c}^2 - f^2}} \frac{\mathbf{c}_0}{\mathbf{c}},\tag{27}$$

we obtain that c^2 must satisfy

$$c^2 > \frac{f^2}{k^2},$$
 (28)

and, as the left-hand side of (27) is positive and $\rho_0 \frac{f^2 |\mathbf{c}|}{\sqrt{k^2 \mathbf{c}^2 - f^2}} > 0$, \mathbf{c}_0 and \mathbf{c} must have the same sign, giving $\mathbf{c} < 0$.

The dispersion relation for the nonlinear waves in (8) and (16) is obtained from the last two

equations in (22) and (24), namely

$$(\rho_1 - \rho_0) \left(bkc^2 + dfc + ga \right) = -\rho_0 dfc_0$$
 (29)

and

$$bkc^2 + ga + dfc = \frac{\rho_2}{\rho_1}ga \tag{30}$$

which are independent of the labeling variables q, r, s.

Rewriting (29) as

$$bkc^{2} + dfc + ga = -\frac{\rho_{0}}{(\rho_{1} - \rho_{0})}dfc_{0}$$
(31)

and equaling the left-hand sides of (30) and (31) we arrive at

$$\frac{\rho_2}{\rho_1}ga = -\frac{\rho_0}{(\rho_1 - \rho_0)}df \mathbf{c}_0 \stackrel{(10)}{=} \frac{\rho_0}{(\rho_1 - \rho_0)} \frac{f^2ma}{k^2} \frac{\mathbf{c}_0}{\mathbf{c}}.$$
 (32)

Defining the reduced gravity g as

$$\mathfrak{g} := \left(\frac{\rho_1 - \rho_0}{\rho_0}\right) \frac{\rho_2}{\rho_1} g,\tag{33}$$

we get, from (32), that

$$g = \frac{f^2 m}{k^2} \frac{c_0}{c}.$$
 (34)

Taking the square of both sides of (34) and making use of (10) we obtain the following dispersion relation

$$c^{2} = \frac{f^{2}}{k^{2}} + \frac{f^{4}c_{0}^{2}}{g^{2}k^{2}} = \frac{f^{2}}{k^{2}} \left(1 + \frac{f^{2}c_{0}^{2}}{g^{2}} \right).$$
 (35)

Observe that (35) satisfies the condition (28), and as we ask for c < 0, we have that

$$c = -\sqrt{\frac{f^2}{k^2} + \frac{f^4 c_0^2}{g^2 k^2}}. (36)$$

Since g is of order of $10^{-3} \div 10^{-4}\,\mathrm{ms^{-2}}$ (see the discussion in Section 4), $f = 2\Omega \approx 1.5 \cdot 10^{-4}\,\mathrm{s^{-1}}$ and $c_0 \lesssim 0.1\,\mathrm{ms^{-1}}$, it follows that

$$c^2 \approx \frac{f^2}{k^2},\tag{37}$$

hence the modulus of the period of the wave $T = \frac{L}{c}$ is approximately $\frac{2\pi}{f} = T_i$, where T_i is the inertial period of the Earth, so the wave motion describing the halocline surfaces is near-inertial.

e. Vorticity and mean velocities

The deep motionless layer beneath the halocline, being in hydrostatic state, is irrotational, whereas in the halocline layer $\mathcal{H}(t)$ and in the layer $\mathcal{M}(t)$ above it the vorticity vector

$$\omega = \left(\frac{\partial w}{\partial y} - \frac{\partial v}{\partial z}, \frac{\partial u}{\partial z} - \frac{\partial w}{\partial x}, \frac{\partial v}{\partial x} - \frac{\partial u}{\partial y}\right) \tag{38}$$

is given by

$$\omega^{T} = \begin{pmatrix} \frac{m^{2}af}{k\Delta} e^{-ms} \sin \Theta \\ \frac{ca(k^{2}-m^{2})\cos\Theta + cma^{2}(m^{2}+k^{2})e^{-ms}}{\Delta} e^{-ms} \\ \frac{fma(\cos\Theta + mae^{-ms})}{\Delta} e^{-ms} \end{pmatrix}, \tag{39}$$

due to the relations

$$\left(\frac{\partial(q,r,s)}{\partial(x,y,z)}\right) \left(\frac{\partial(u,v,w)}{\partial(q,r,s)}\right) = \left(\frac{\partial(u,v,w)}{\partial(x,y,z)}\right),
\left(\frac{\partial(q,r,s)}{\partial(x,y,z)}\right) = \left(\frac{\partial(x,y,z)}{\partial(q,r,s)}\right)^{-1},$$
(40)

with

$$\left(\frac{\partial(q,r,s)}{\partial(x,y,z)}\right) = \begin{pmatrix} q_x & r_x & s_x \\ q_y & r_y & s_y \\ q_z & r_z & s_z \end{pmatrix} =
= \frac{1}{\Delta} \begin{pmatrix} 1 + ma e^{-ms} \cos\Theta & \frac{fma e^{-ms} \sin\Theta}{kc} & -kae^{-ms} \sin\Theta \\ 0 & \Delta & 0 \\ -\frac{m^2 a e^{-ms} \sin\Theta}{k} & \frac{fm^2 a e^{-ms} \cos\Theta - m^3 a^2 f e^{-2ms}}{k^2 c} & 1 - ma e^{-ms} \cos\Theta \end{pmatrix}, \tag{41}$$

where $\Delta = 1 - m^2 a^2 e^{-2ms}$ is the determinant given in (13).

The velocity gradient tensor, which is the same in the two layers $\mathcal{H}(t)$ and $\mathcal{M}(t)$, is given by

$$\nabla \mathbf{U} = \begin{pmatrix} U_{x} & U_{y} & U_{z} \\ V_{x} & V_{y} & V_{z} \\ W_{x} & W_{y} & W_{z} \end{pmatrix} = \begin{pmatrix} U_{q} & U_{r} & U_{s} \\ V_{q} & V_{r} & V_{s} \\ W_{q} & W_{r} & W_{s} \end{pmatrix} \begin{pmatrix} q_{x} & r_{x} & s_{x} \\ q_{y} & r_{y} & s_{y} \\ q_{z} & r_{z} & s_{z} \end{pmatrix} =$$

$$= \frac{1}{\Delta} \begin{pmatrix} -mack \ e^{-ms} \sin\Theta & 0 \ m^{2}ac \ e^{-ms} (ma \ e^{-ms} - \cos\Theta) \\ fma \ e^{-ms} (\cos\Theta + ma \ e^{-ms}) & 0 \ -\frac{fm^{2}a}{k} e^{-ms} \sin\Theta \\ -k^{2}ca \ e^{-ms} (\cos\Theta + ma \ e^{-ms}) & 0 \ kmca \ e^{-ms} \sin\Theta \end{pmatrix},$$
(42)

making use of (41) and the formulae

$$U_{q} = -kamc e^{-ms} \sin\Theta, \qquad U_{r} = 0, \qquad U_{s} = -am^{2}c e^{-ms} \cos\Theta,$$

$$V_{q} = fma e^{-ms} \cos\Theta, \qquad V_{r} = 0, \qquad V_{s} = -f\frac{am^{2}}{k} e^{-ms} \sin\Theta,$$

$$W_{q} = -k^{2}ca e^{-ms} \cos\Theta, \qquad W_{r} = 0, \qquad W_{s} = kmca e^{-ms} \sin\Theta.$$

$$(43)$$

From (42), it is immediate to see that

$$U_x = -W_z, \qquad V_x = -\frac{fm}{k^2 \mathbf{c}} W_x \qquad \text{and} \qquad V_z = -\frac{fm}{k^2 \mathbf{c}} W_z.$$
 (44)

Before proceeding with the stability analysis, we recall some mean-flow properties of the fluid motion described by (8) and (16), referring to (Puntini 2025a) for more details (see also (Kluczek 2018; Kluczek and Stuhlmeier 2020)).

In the halocline layer $\mathcal{H}(t)$, the mean Lagrangian velocities over a wave period $T = \frac{L}{c}$ are given by

$$\langle U \rangle_{L} = \frac{1}{T} \int_{0}^{T} U(q - ct, r, s) dt = 0,$$

$$\langle V \rangle_{L} = \frac{1}{T} \int_{0}^{T} V(q - ct, r, s) dt = 0,$$

$$\langle W \rangle_{L} = \frac{1}{T} \int_{0}^{T} W(q - ct, r, s) dt = 0,$$

$$(45)$$

whereas in the layer $\mathcal{M}(t)$ above the halocline:

$$\langle U \rangle_L = -\mathbf{c}_0, \qquad \langle V \rangle_L = 0, \qquad \langle W \rangle_L = 0.$$
 (46)

The mean Lagrangian velocity is also called mass-transport velocity, as it is the mean velocity of a marked particle (cf. (Longuet-Higgins 1969; Constantin 2013)).

In the halocline layer $\mathcal{H}(t)$, the mean Eulerian velocities at a fixed depth z_0 are given by

$$\langle U \rangle_{E}(z_{0}) = \frac{1}{T} \int_{0}^{T} U(x - ct, y, z) dt = -\frac{m^{2} a^{2} c}{L} \int_{0}^{L} e^{-2mS} dq,$$

$$\langle V \rangle_{E}(z_{0}) = \frac{1}{T} \int_{0}^{T} V(x - ct, y, z) dt = \frac{f m a}{k L} \int_{0}^{L} e^{-mS} (\sin \Theta) \frac{1 - m^{2} a^{2} e^{-2mS}}{1 + m a e^{-mS} \cos \Theta} dq,$$

$$\langle W \rangle_{E}(z_{0}) = \frac{1}{T} \int_{0}^{T} W(x - ct, y, z) dt = -\frac{k ca}{L} \int_{0}^{L} e^{-mS} (\sin \Theta) \frac{1 - m^{2} a^{2} e^{-2mS}}{1 + m a e^{-mS} \cos \Theta} dq,$$

$$(47)$$

where

$$z_0 = -d_0 + s - ae^{-ms}\cos\Theta \tag{48}$$

and S comes from the relation (48) written in implicit form as $s = S(z_0, \Theta)$ (see (Puntini 2025a) for more details).

In the layer $\mathcal{M}(t)$ we have that

$$\langle U \rangle_E(z_0) = -\frac{m^2 a^2 c}{L} \int_0^L e^{-2mS} dq - \frac{c_0}{L} \int_0^L \frac{1 - m^2 a^2 e^{-2mS}}{1 + mae^{-mS} \cos \Theta} dq, \tag{49}$$

whereas $\langle V \rangle_E(z_0)$ and $\langle W \rangle_E(z_0)$ are the same as in (47).

3. Instability

In this section, we first recall the short-wavelength instability approach for geophysical flows (see e.g. Constantin and Germain (2013); Ionescu-Kruse (2016b, 2017)), and then we apply it to the near-inertial Pollard waves for the 3-layer model describing the arctic halocline under consideration.

a. Short-wavelength instability approach

Small perturbations $\mathbf{u}(\mathbf{X},t)$, $p(\mathbf{X},t)$ of the basic flow $\mathbf{U}(\mathbf{X},t)$, $P(\mathbf{X},t)$ are governed by the following linearized equations

$$\begin{cases}
\mathbf{u}_{t} + (\mathbf{U} \cdot \nabla)\mathbf{u} + (\mathbf{u} \cdot \nabla)\mathbf{U} + \mathcal{L}\mathbf{u} = -\frac{1}{\rho}\nabla p, \\
\nabla \cdot \mathbf{u} = 0,
\end{cases}$$
(50)

where

$$\mathcal{L} = \begin{pmatrix} 0 & -f & 0 \\ f & 0 & 0 \\ 0 & 0 & 0 \end{pmatrix},\tag{51}$$

and, for the analysis of the flow we will set $\rho = \rho_0$ or $\rho = \rho_1$, depending on the layer under consideration.

The short-wavelength instability approach consists in the study of the evolution in time of the solutions of the linearized system (50) in the following WKB form

$$\mathbf{u}(\mathbf{X},t) = \left[\mathbf{A}(\mathbf{X},t) + \epsilon \mathcal{A}(\mathbf{X},t)\right] e^{\frac{i}{\epsilon}\Phi(\mathbf{X},t)} + \epsilon \mathbf{u}_{rem}(\mathbf{X},t,\epsilon),$$

$$p(\mathbf{X},t) = \left[B(\mathbf{X},t) + \epsilon \mathcal{B}(\mathbf{X},t)\right] e^{\frac{i}{\epsilon}\Phi(\mathbf{X},t)} + \epsilon p_{rem}(\mathbf{X},t,\epsilon),$$
(52)

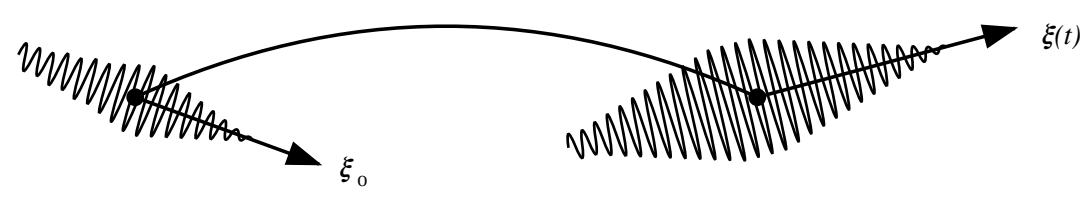
where ϵ is a small parameter, **A** and \mathcal{A} are vector functions, while Φ , B and \mathcal{B} are scalar functions, and with the initial condition

$$\mathbf{u}_0 := \mathbf{u}(\mathbf{X}, 0) = \mathbf{A}(\mathbf{X}, 0) e^{\frac{i}{\epsilon} \Phi(\mathbf{X}, 0)}$$
(53)

representing a sharply-peaked initial disturbance.

Substituting the expression for \mathbf{u} and p given by (52) into the linearized equations (50), we get

Lagrangian trajectory of the basic flow



wave-packet localized around X_0

wave-packet localized around $X(X_0, t)$

Fig. 5. Evolution of a high-frequency wavelet disturbance along the basic flow.

$$\begin{cases} \frac{i}{\epsilon} e^{\frac{i}{\epsilon}\Phi} (\Phi_{t} + \mathbf{U} \cdot \Phi) \mathbf{A} + e^{\frac{i}{\epsilon}\Phi} (\mathbf{A}_{t} + (\mathbf{U} \cdot \nabla) \mathbf{A} + (\mathbf{A} \cdot \nabla) \mathbf{U} + \mathcal{L} \mathbf{A} + i\mathcal{H}(\Phi_{t} + \mathbf{U} \cdot \Phi)) + \\ + \epsilon \left[e^{\frac{i}{\epsilon}\Phi} (\mathcal{H}_{t} + (\mathbf{U} \cdot \nabla)\mathcal{H} + (\mathcal{H} \cdot \nabla) \mathbf{U} + \mathcal{L} \mathbf{A}) + (\mathbf{u}_{rem})_{t} + (\mathbf{U} \cdot \nabla) \mathbf{u}_{rem} + (\mathbf{u}_{rem} \cdot \nabla) \mathbf{U} + p \mathbf{u}_{rem} \right] = \\ = -\frac{i}{\epsilon} e^{\frac{i}{\epsilon}\Phi} \frac{B}{\rho} \nabla \Phi - e^{\frac{i}{\epsilon}\Phi} \left[\nabla \left(\frac{B}{\rho} \right) + i \frac{\mathcal{B}}{\rho} \nabla \Phi \right] - \epsilon \left[e^{\frac{i}{\epsilon}\Phi} \nabla \left(\frac{\mathcal{B}}{\rho} \right) + \nabla \left(\frac{p_{rem}}{\rho} \right) \right], \\ \frac{i}{\epsilon} e^{\frac{i}{\epsilon}\Phi} (\mathbf{A} \cdot \nabla \Phi) + e^{\frac{i}{\epsilon}\Phi} (\nabla \cdot \mathbf{A} + i\mathcal{H} \cdot \nabla \Phi) + \epsilon \left[e^{\frac{i}{\epsilon}\Phi} (\nabla \cdot \mathcal{H} + \nabla \cdot \mathbf{u}_{rem}) \right] = 0, \end{cases}$$

$$(54)$$

and equating the terms with same order in ϵ , we obtain the expressions for A, \mathcal{A} , Φ , B, \mathcal{B} (see e.g. (Constantin and Germain 2013; Miao et al. 2022) for the details):

$$\mathbf{A} \cdot \nabla \Phi = 0, \tag{55}$$

$$\nabla \cdot \mathbf{A} + i\mathcal{H} \cdot \nabla \Phi = 0, \tag{56}$$

$$(\Phi_t + \mathbf{U} \cdot \Phi)\mathbf{A} = -\frac{B}{\rho} \nabla \Phi, \tag{57}$$

$$\mathbf{A}_{t} + (\mathbf{U} \cdot \nabla)\mathbf{A} + (\mathbf{A} \cdot \nabla)\mathbf{U} + \mathcal{L}\mathbf{A} + i\mathcal{A}(\Phi_{t} + \mathbf{U} \cdot \Phi) = -\left[\nabla\left(\frac{B}{\rho}\right) + i\frac{\mathcal{B}}{\rho}\nabla\Phi\right]. \tag{58}$$

For all $\mathbf{A} \neq 0$ and $\mathbf{\Phi} \neq 0$, from (55), (56) and (57) we get

$$B = 0, (59)$$

$$\Phi_t + \mathbf{U} \cdot \nabla \Phi = 0, \tag{60}$$

and from (56) and (58) it follows that

$$\mathcal{A} = i \frac{(\nabla \cdot \mathbf{A}) \nabla \Phi}{||\nabla \Phi||^2},\tag{61}$$

$$\mathcal{B} = i\rho \frac{\nabla \Phi \cdot [2(\mathbf{A} \cdot \nabla)\mathbf{U} + \mathcal{L}\mathbf{A}]}{||\nabla \Phi||^2},\tag{62}$$

where $||\cdot||$ denotes the standard L^2 -norm.

Summing up, we obtain the following system governing the evolution of the short-wavelength perturbation at leading order in power of ϵ

$$\Phi_t + \mathbf{U} \cdot \nabla \Phi = 0, \tag{63}$$

$$\mathbf{A}_{t} + (\mathbf{U} \cdot \nabla)\mathbf{A} + (\mathbf{A} \cdot \nabla)\mathbf{U} + \mathcal{L}\mathbf{A} = \frac{\nabla \Phi \cdot [2(\mathbf{A} \cdot \nabla)\mathbf{U} + \mathcal{L}\mathbf{A}]}{||\nabla \Phi||^{2}} \nabla \Phi, \tag{64}$$

consisting of an eikonal equation and a transport equation, and with the initial conditions

$$\Phi(\mathbf{X},0) = \Phi_0(\mathbf{X}), \qquad \mathbf{A}(\mathbf{X},0) = \mathbf{A}_0(\mathbf{X}) \tag{65}$$

satisfying

$$\mathbf{A}_0 \cdot \nabla \Phi_0 = 0. \tag{66}$$

For the reminder terms \mathbf{u}_{rem} and p_{rem} , which are not necessary for the instability analysis we are performing, we remark that they are bounded, in an appropriate norm, at any time t by functions that can depend on t but not on ϵ , thus can be neglected as $\epsilon \to 0$ (see (Ionescu-Kruse 2016a,b, 2015c)).

The trajectory of U through a point X_0 is given by

$$\begin{cases} \frac{D\mathbf{X}}{Dt} = \mathbf{U}(\mathbf{X}, t), \\ \mathbf{X}(0) = \mathbf{X}_0. \end{cases}$$
(67)

Observe that the eikonal and transport equations in (63) and (64) can be solved independently along the streamlines, as they involve only the advective derivative of the basic velocity field **U**. Writing $\xi = \nabla \Phi$, taking the gradient of (63) we have that

$$\boldsymbol{\xi}_t + (\mathbf{U} \cdot \nabla)\boldsymbol{\xi} + (\nabla \mathbf{U})^T \boldsymbol{\xi} = 0, \tag{68}$$

namely

$$\frac{D\boldsymbol{\xi}}{Dt} = -(\nabla \mathbf{U})^T \boldsymbol{\xi} \tag{69}$$

with the initial condition $\xi(0) = \xi_0$ and where $\nabla \mathbf{U}$ is given by

$$\nabla \mathbf{U} = \begin{pmatrix} U_x & U_y & U_z \\ V_x & V_y & V_z \\ W_x & W_y & W_z \end{pmatrix}. \tag{70}$$

Moreover, writing $\mathbf{A} = (A_1, A_2, A_3)$, (64) reads as

$$\frac{D\mathbf{A}}{Dt} = -(\mathbf{A} \cdot \nabla)\mathbf{U} - \mathcal{L}\mathbf{A} + \frac{\boldsymbol{\xi} \cdot [2(\mathbf{A} \cdot \nabla)\mathbf{U} + \mathcal{L}\mathbf{A}]}{||\boldsymbol{\xi}||^2} \boldsymbol{\xi}$$
(71)

with the initial condition $A(0) = A_0$.

Therefore, we can conclude that the evolution in time of X, ξ and A, at leading order, is given by the following coupled system of ODEs

$$\begin{cases} \frac{D\mathbf{X}}{Dt} = \mathbf{U}(\mathbf{X}, t), \\ \frac{D\boldsymbol{\xi}}{Dt} = -(\nabla \mathbf{U})^T \boldsymbol{\xi}, \\ \frac{D\mathbf{A}}{Dt} = -(\mathbf{A} \cdot \nabla)\mathbf{U} - \mathcal{L}\mathbf{A} + \frac{\boldsymbol{\xi} \cdot [2(\mathbf{A} \cdot \nabla)\mathbf{U} + \mathcal{L}\mathbf{A}]}{||\boldsymbol{\xi}||^2} \boldsymbol{\xi}, \end{cases}$$
(72)

with associated initial conditions

$$\mathbf{X}(0) = \mathbf{X}_0, \qquad \boldsymbol{\xi}(0) = \boldsymbol{\xi}_0, \qquad \mathbf{A}(0) = \mathbf{A}_0,$$
 (73)

satisfying the constraint

$$\mathbf{A}_0 \cdot \boldsymbol{\xi}_0 = 0. \tag{74}$$

The first equation in (72) describes the particle trajectory of the basic flow, while the second and third govern - at leading order - the evolution of the local wave vector and the amplitude of the perturbation along the particle trajectory, respectively. The growth rate of \mathbf{A} is analogous to the concept of Lyapunov exponent (see e.g. Friedlander and Yudovich (1999); Constantin and Germain (2013); Henry and Hsu (2015)). If fore some initial position \mathbf{X}_0 we have that

$$\Lambda(\mathbf{X}_0) = \limsup_{t \to \infty} \frac{1}{t} \ln \left(\sup_{\substack{|\boldsymbol{\xi}_0| = |\mathbf{A}_0| = 1\\ \boldsymbol{\xi}_0 \cdot \mathbf{A}_0 = 0}} |\mathbf{A}(\mathbf{X}, t; \boldsymbol{\xi}_0, \mathbf{A}_0)| \right) > 0$$
 (75)

then, for a given fluid trajectory, the particles separate at an exponential rate, and the fluid flow is unstable (Friedlander and Yudovich 1999). This is associated to the fact that - in the spectral analysis framework - the unbounded operator associated to the linearization around the basic flow has a nonempty unstable continuous spectrum in L^2 (see (Constantin and Germain 2013; Friedlander and Yudovich 1999)).

b. Instability of the halocline

In order to prove the instability of the Pollard waves in (8) and (16) it is not necessary to investigate the system (72) for all the initial data. Instead, it is sufficient to provide one initial disturbance resulting in an exponential growth of \mathbf{A} . With this scope, we choose the following initial wave vector

$$\boldsymbol{\xi}_0 = \left(0, \frac{k}{m}, \frac{f}{kc}\right),\tag{76}$$

and it can be proven that a solution to $\frac{D\xi}{Dt} = -(\nabla \mathbf{U})^T \boldsymbol{\xi}$ is given by (see (Ionescu-Kruse 2016b) for the details)

$$\boldsymbol{\xi}(t) = \begin{pmatrix} \Xi_{11} & \Xi_{12} & \Xi_{13} \\ 0 & 1 & 0 \\ \Xi_{31} & \Xi_{32} & \Xi_{33} \end{pmatrix} \boldsymbol{\xi}_0 \tag{77}$$

where

$$\Xi_{11} = 1 + ma e^{-ms} (\cos \Theta - \cos(kq)) - m^{2} a^{2} e^{-2ms} \cos(kct),
\Xi_{12} = \frac{f}{kc} \left[ma e^{-ms} (\sin \Theta - \sin(kq)) - m^{2} a^{2} e^{-2ms} \sin(kct) \right],
\Xi_{13} = ka e^{-ms} (\sin(kq) - \sin \Theta) + mk a^{2} e^{-2ms} \sin(kct),
\Xi_{31} = \frac{m^{2} a}{k} e^{-ms} (\sin(kq) - \sin \Theta) - \frac{m^{3} a^{2}}{k} e^{-2ms} \sin(kct),
\Xi_{32} = \frac{f}{k^{2}c} \left[m^{3} a^{2} e^{-2ms} (\cos(kct) - 1) + m^{2} a e^{-ms} (\cos \Theta - \cos(kq)) \right],
\Xi_{33} = 1 - m^{2} a^{2} e^{-2ms} \cos(kct) - ma e^{-ms} (\cos \Theta - \cos(kq)),$$
(78)

from which it follows that

$$\xi(t) = \left(0, \frac{k}{m}, \frac{f}{kc}\right) \qquad \forall t \ge 0. \tag{79}$$

Inserting the expression (42) for $\nabla \mathbf{U}$ and the above one for $\boldsymbol{\xi}(t)$ into the third equation of (72) governing the time evolution of the amplitude of the disturbance \mathbf{A} we get

$$\frac{D\mathbf{A}}{Dt} = \underbrace{\begin{pmatrix} -U_x & f & -U_z \\ \frac{fm}{k^2c}W_x - \frac{f^3}{k^2c^2} & 0 & \frac{fm}{k^2c}W_z \\ -W_x + \frac{f^2}{cm} & 0 & -W_z \end{pmatrix}}_{:=M(t)} \begin{pmatrix} A_1 \\ A_2 \\ A_3 \end{pmatrix} \tag{80}$$

where we used (44) to simplify the expressions in the matrix M(t), as well as (10) to write

$$\frac{f^2 m^2}{f^2 m^2 + k^4 \mathbf{c}^2} = \frac{f^2 k^4 \mathbf{c}^2}{k^2 \mathbf{c}^2 - f^2} \frac{1}{\frac{f^2 k^4 \mathbf{c}^2}{k^2 \mathbf{c}^2 - f^2} + k^4 \mathbf{c}^2} = \frac{f^2}{k^2 \mathbf{c}^2}.$$
 (81)

For completeness, the explicit form of M(t) is

$$M(t) = \begin{pmatrix} \frac{macke^{-ms}}{\Delta}\sin\Theta & f & -\frac{m^2ac}{\Delta}e^{-ms}(mae^{-ms} - \cos\Theta) \\ -\frac{fma}{\Delta}e^{-ms}(cos\Theta + mae^{-ms}) - \frac{f^3}{k^2c^2} & 0 & \frac{fm^2a}{k\Delta}e^{-ms}\sin\Theta \\ \frac{k^2ca}{\Delta}e^{-ms}(cos\Theta + mae^{-ms}) + \frac{f^2}{cm} & 0 & -\frac{kmca}{\Delta}e^{-ms}\sin\Theta \end{pmatrix}.$$
(82)

Multiplying the last equation of (80) by $\frac{fm}{kc^2}$ and summing it to the second one we get

$$\frac{dA_2(t)}{dt} = -\frac{fm}{k^2 c} \frac{dA_3(t)}{dt},\tag{83}$$

which gives

$$A_2(t) = -\frac{fm}{k^2 \mathbf{c}} A_3(t) \tag{84}$$

if we choose the initial condition $A_2(0) = 0$, and, recalling the constraint (74)

$$\mathbf{A}_0 \cdot \boldsymbol{\xi}_0 = 0, \tag{85}$$

and that

$$\xi(t) = \left(0, \frac{k}{m}, \frac{f}{kc}\right) \qquad \forall t \ge 0$$
 (86)

it follows that A_0 should have the form $(a_1, 0, 0)$ with $a_1 \in \mathbb{R}$. Therefore, the most natural choice is $A_0 = (1, 0, 0)$ (which verifies (84)).

The linear system (80) is non-autonomous as Θ depends on t. We transform it into an autonomous one by rotating the canonical basis by an angle

$$\beta = -\frac{kct}{2} \tag{87}$$

about the vector $\left(0, \frac{k}{m}, \frac{f}{kc}\right)$. The rotation matrix (due to the Rodrigues formula (Cheng and Gupta 1989)) is given by

$$\mathcal{R}(t) = \begin{pmatrix} \cos \beta & -\frac{f}{kc} \sin \beta & \frac{k}{m} \sin \beta \\ \frac{f}{kc} \sin \beta & 1 - \frac{f^2}{k^2 c^2} (1 - \cos \beta) & \frac{f}{cm} (1 - \cos \beta) \\ -\frac{k}{m} \sin \beta & \frac{f}{cm} (1 - \cos \beta) & 1 - \frac{k^2}{m^2} (1 - \cos \beta) \end{pmatrix}$$
(88)

with inverse

$$\mathcal{R}^{-1}(t) = \mathcal{R}^{T}(t) = \begin{pmatrix} \cos \beta & \frac{f}{kc} \sin \beta & -\frac{k}{m} \sin \beta \\ -\frac{f}{kc} \sin \beta & 1 - \frac{f^{2}}{k^{2}c^{2}} (1 - \cos \beta) & \frac{f}{cm} (1 - \cos \beta) \\ \frac{k}{m} \sin \beta & \frac{f}{cm} (1 - \cos \beta) & 1 - \frac{k^{2}}{m^{2}} (1 - \cos \beta) \end{pmatrix}.$$
(89)

The the components $(Q_1(t), Q_2(t), Q_3(t))$ of the vector $\mathbf{A}(t)$ in the new basis are related to the components in the canonical basis, namely $(A_1(t), A_2(t), A_3(t))$, by

$$\begin{pmatrix}
Q_1(t) \\
Q_2(t) \\
Q_3(t)
\end{pmatrix} = \mathcal{R}^{-1}(t) \begin{pmatrix}
A_1(t) \\
A_2(t) \\
A_3(t)
\end{pmatrix}.$$
(90)

Even if $(Q_1(t), Q_2(t), Q_3(t))$ and $(A_1(t), A_2(t), A_3(t))$ represent the same vector $\mathbf{A}(t)$ in two different basis, with abuse of notation we write $\mathbf{Q}(t) = (Q_1(t), Q_2(t), Q_3(t))$ and $\mathbf{A}(t) = (A_1(t), A_2(t), A_3(t))$. From (84) and (90) it follows that

$$Q_2(t) = -\frac{fm}{k^2 c} Q_3(t) \qquad \text{for all } t \ge 0.$$
 (91)

Differentiating with respect to time (90) and making use of (80) we get

$$\frac{d\mathbf{Q}}{dt} = \underbrace{\left[\frac{d\mathcal{R}^T}{dt}\mathcal{R}(t) + \mathcal{R}^T(t)M(t)\mathcal{R}(t)\right]}_{:-\mathcal{E}}\mathbf{Q}(t)$$
(92)

where we used the fact that $\mathcal{R}^{-1}(t) = \mathcal{R}^{T}(t)$. Taking the time derivative of the matrix (89) leads to

$$\frac{d\mathcal{R}^{T}}{dt} = \begin{pmatrix}
\frac{k\mathbf{c}}{2}\sin\beta & -\frac{f}{2}\cos\beta & \frac{k^{2}\mathbf{c}}{2m}\cos\beta \\
\frac{f}{2}\cos\beta & \frac{f^{2}}{2k\mathbf{c}}\sin\beta & -\frac{fk}{2m}\sin\beta \\
-\frac{k^{2}\mathbf{c}}{2m}\cos\beta & -\frac{fk}{2m}\sin\beta & \frac{k^{3}\mathbf{c}}{2m^{2}}\sin\beta
\end{pmatrix}, \tag{93}$$

and, consequently,

$$\frac{d\mathcal{R}^{T}}{dt}\mathcal{R}(t) = \begin{pmatrix} 0 & -\frac{f}{2} & \frac{k^{2}c}{2m} \\ \frac{f}{2} & 0 & 0 \\ -\frac{k^{2}c}{2m} & 0 & 0 \end{pmatrix}.$$
(94)

Moreover, note that the matrix M(t) can be written in the following compact form

$$M(t) = \begin{pmatrix} -M_{33} & M_{12} & M_{13} \\ -\frac{fm}{k^2c}M_{31} & 0 & -\frac{fm}{k^2c}M_{33} \\ M_{31} & 0 & M_{33} \end{pmatrix}$$
(95)

where (cf. (44) and (80))

$$M_{13} = -U_z$$
, $M_{33} = -W_z$, $M_{12} = f$, $M_{31} = -W_x + \frac{f^2}{cm}$. (96)

Due to (91) we can rewrite the system (92) as the following planar system

$$\begin{pmatrix}
\frac{dQ_1}{dt} \\
\frac{dQ_3}{dt}
\end{pmatrix} = \underbrace{\begin{pmatrix}
\mathcal{E}_{11} & -\frac{fm}{k^2c}\mathcal{E}_{12} + \mathcal{E}_{13} \\
\mathcal{E}_{31} & -\frac{fm}{k^2c}\mathcal{E}_{32} + \mathcal{E}_{33}
\end{pmatrix}}_{:=\Pi} \begin{pmatrix}
Q_1 \\
Q_3
\end{pmatrix}, \tag{97}$$

and, calling $P(t) = \mathcal{R}^T(t)M(t)$ and $S(t) = \mathcal{R}^T(t)M(t)\mathcal{R}(t)$ we have

$$S_{11} = P_{11}\mathcal{R}_{11} + P_{12}\mathcal{R}_{21} + P_{13}\mathcal{R}_{31} = \frac{kmca}{\Delta}e^{-ms}\sin(kq),$$

$$-\frac{fm}{k^{2}c}S_{12} + S_{13} = P_{11}\left(-\frac{fm}{k^{2}c}\mathcal{R}_{12} + \mathcal{R}_{13}\right) + P_{12}\left(-\frac{fm}{k^{2}c}\mathcal{R}_{22} + \mathcal{R}_{23}\right) + P_{13}\left(-\frac{fm}{k^{2}c}\mathcal{R}_{32} + \mathcal{R}_{33}\right)$$

$$= \frac{m^{2}ca}{\Delta}e^{-ms}\cos(kq) - \frac{f^{2}m}{k^{2}c} - \frac{m^{3}ca^{2}}{\Delta}e^{-2ms},$$

$$S_{31} = P_{31}\mathcal{R}_{11} + P_{32}\mathcal{R}_{21} + P_{33}\mathcal{R}_{31} = \frac{k^{2}ca}{\Delta}e^{-ms}\cos(kq) + \frac{f^{2}}{cm} + \frac{k^{2}cma^{2}}{\Delta}e^{-2ms},$$

$$-\frac{fm}{k^{2}c}S_{32} + S_{33} = P_{31}\left(-\frac{fm}{k^{2}c}\mathcal{R}_{12} + \mathcal{R}_{13}\right) + P_{32}\left(-\frac{fm}{k^{2}c}\mathcal{R}_{22} + \mathcal{R}_{23}\right) + P_{33}\left(-\frac{fm}{k^{2}c}\mathcal{R}_{32} + \mathcal{R}_{33}\right)$$

$$= -\frac{kmca}{\Delta}e^{-ms}\sin(kq),$$

$$(98)$$

where

$$P_{11} = -M_{33}\cos\beta - \frac{m}{k}M_{31}\sin\beta, \qquad P_{12} = f\cos\beta, \qquad P_{13} = M_{13}\cos\beta - \frac{m}{k}M_{33}\sin\beta,$$

$$P_{21} = \frac{f}{kc}M_{33}\sin\beta - \frac{fm}{k^2c}M_{31}\cos\beta, \qquad P_{22} = -\frac{f^2}{kc}\sin\beta, \qquad P_{23} = -\frac{f}{kc}M_{13}\sin\beta - \frac{fm}{k^2c}M_{33}\cos\beta, \qquad (99)$$

$$P_{31} = -\frac{k}{m}M_{33}\sin\beta + M_{31}\cos\beta, \qquad P_{32} = \frac{fk}{m}\sin\beta, \qquad P_{33} = \frac{k}{m}M_{13}\sin\beta + M_{33}\cos\beta.$$

Summing up, due to (94) and (98), the planar system (97) reads as

$$\begin{pmatrix}
\frac{dQ_1}{dt} \\
\frac{dQ_3}{dt}
\end{pmatrix} = \Pi \begin{pmatrix} Q_1 \\
Q_3 \end{pmatrix},$$
(100)

where Π is the following 2×2 time-independent matrix

$$\Pi = \left(\frac{\frac{kmca}{\Delta}e^{-ms}\sin(kq)}{\frac{k^{2}ca}{\Delta}e^{-ms}\cos(kq) + \frac{k^{2}c^{2}m - 2f^{2}m}{2k^{2}c} - \frac{m^{3}ca^{2}}{\Delta}e^{-2ms}}{\frac{k^{2}ca}{\Delta}e^{-ms}\cos(kq) + \frac{k^{2}c^{2}m - 2f^{2}m}{2k^{2}c} - \frac{m^{3}ca^{2}}{\Delta}e^{-2ms}}{\frac{k^{2}ca}{\Delta}e^{-ms}\sin(kq)} \right). \tag{101}$$

Since $Tr(\Pi) = 0$, the eigenvalues of Π are given by

$$\lambda_{\pm} = \pm \sqrt{-\text{Det}(\Pi)},\tag{102}$$

with

$$Det(\Pi) = -\frac{k^2 m^2 c^2 a^2}{\Delta} e^{-2ms} + \left(\frac{k^2 c^2 - 2f^2}{2kc}\right)^2,$$
 (103)

leading to

$$\lambda_{\pm} = \pm \sqrt{\frac{k^2 m^2 c^2 a^2}{\Delta} e^{-2ms} - \left(\frac{k^2 c^2 - 2f^2}{2kc}\right)^2};$$
(104)

therefore, as the rotation matrix $\mathcal{R}(t)$ is time-periodic, the time evolution of the amplitude vector $\mathbf{A}(t)$ is determined by the eigenvalues of the matrix Π . If λ_+ is real and positive, an exponential growth of $\mathbf{A}(t)$ will occur, with growth rate λ_+ . Recalling that $\Delta = 1 - m^2 a^2 e^{-2ms} > 0$, λ_+ is real and positive if and only if

$$m^{2}a^{2}e^{-2ms} > \frac{(k^{2}c^{2} - 2f^{2})^{2}}{\left[4k^{4}c^{4} + (k^{2}c^{2} - 2f^{2})^{2}\right]}.$$
(105)

The wave height in (8) and (16) is $2a e^{-ms}$, and the wave steepness, defined as the amplitude of the wave multiplied by the wave number k, is equal to $ka e^{-ms}$. Recalling the relation $m^2 = \frac{k^4 c^2}{k^2 c^2 - f^2}$ in (10), the inequality (105) reads as

$$k^{2}a^{2}e^{-2ms} > \frac{k^{2}c^{2} - f^{2}}{k^{2}c^{2}} \frac{(k^{2}c^{2} - 2f^{2})^{2}}{\left[4k^{4}c^{4} + (k^{2}c^{2} - 2f^{2})^{2}\right]}.$$
 (106)

Therefore, if the square of the steepness of the waves described in (8) and (16) satisfies (106), these are unstable, as a small perturbation of the flow will grow exponentially. One of the key features of the nonlinear waves solution (8) and (16) developed in Puntini (2025a) is its simple and explicit dispersion relation (35) (conversely to 2-layers model where the dispersion relation is not explicit and complicated, see e.g. (Constantin and Monismith 2017; McCarney 2023, 2024)). Inserting the dispersion relation (35)

$$c^{2} = \frac{f^{2}}{k^{2}} + \frac{f^{4}c_{0}^{2}}{g^{2}k^{2}} = \frac{f^{2}}{k^{2}} \left(1 + \frac{f^{2}c_{0}^{2}}{g^{2}} \right) \quad \text{with} \quad g \stackrel{(33)}{=} \left(\frac{\rho_{1} - \rho_{0}}{\rho_{0}} \right) \frac{\rho_{2}}{\rho_{1}} g, \quad (107)$$

into (106) we get the following condition for the instability

$$k^{2}a^{2}e^{-2ms} > \frac{f^{2}c_{0}^{2}}{(g^{2} + f^{2}c_{0}^{2})} \frac{(f^{2}c_{0}^{2} - g^{2})^{2}}{\left[5f^{4}c_{0}^{4} + 5g^{4} + 6f^{2}c_{0}^{2}g^{2}\right]} := \mathcal{F}(g, c_{0}), \tag{108}$$

with the right-hand side (denoted by \mathcal{T}) depending only on physical constants $f = 2\Omega \approx 1.5 \cdot 10^{-4} \, \mathrm{s}^{-1}$ and $g = 9.81 \, \mathrm{ms}^{-2}$ and characteristics of the flow: \mathbf{c}_0 , and ρ_0 , ρ_1 and ρ_2 (via $\mathfrak{g} = \left(\frac{\rho_1 - \rho_0}{\rho_0}\right) \frac{\rho_2}{\rho_1} g$). See Fig. 6 and Fig. 7 for plots of \mathcal{T} as a function of \mathfrak{g} and \mathbf{c}_0 .

4. Discussion

We now conclude with some quantitative considerations about the instability threshold in (108). The explicit dispersion relation (35) allows to easily compute the threshold as a function of the water properties: the densities of the three layers and the mean current above the halocline. With this scope, we fix values of the characteristic of the water in the central part of the Arctic Ocean based on (Rudels and Carmack 2022):

• Surface Mixed Layer: water density ρ_0 , $\mathfrak{T} = -1.5^{\circ}$ C, $\mathfrak{S} = 34.0$ psu;

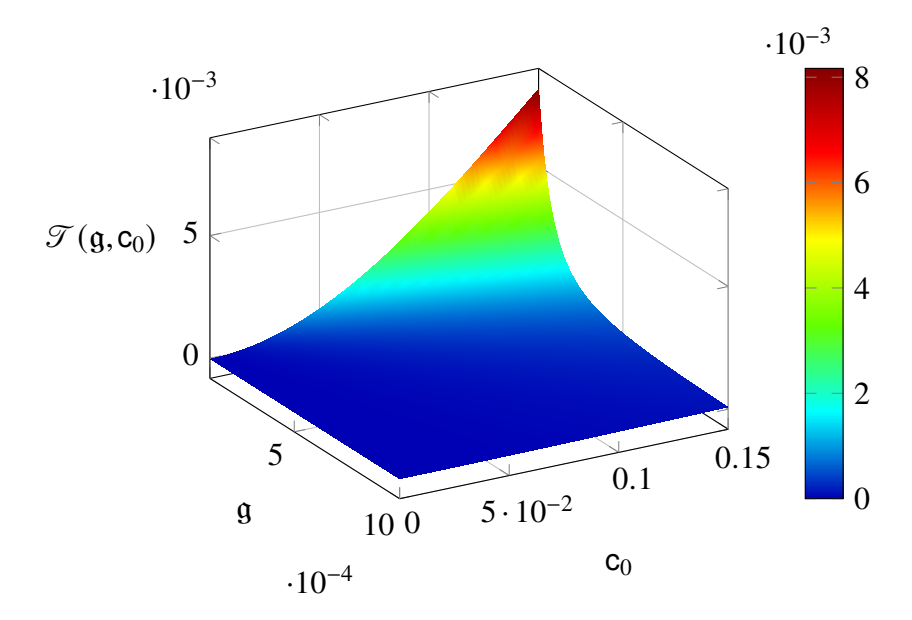


Fig. 6. The treshold \mathcal{T} as a function of \mathfrak{g} and \mathfrak{c}_0 , with $\mathfrak{g} \in [10^{-4}, 10^{-3}]$ and $\mathfrak{c}_0 \in [0, 0.15]$.

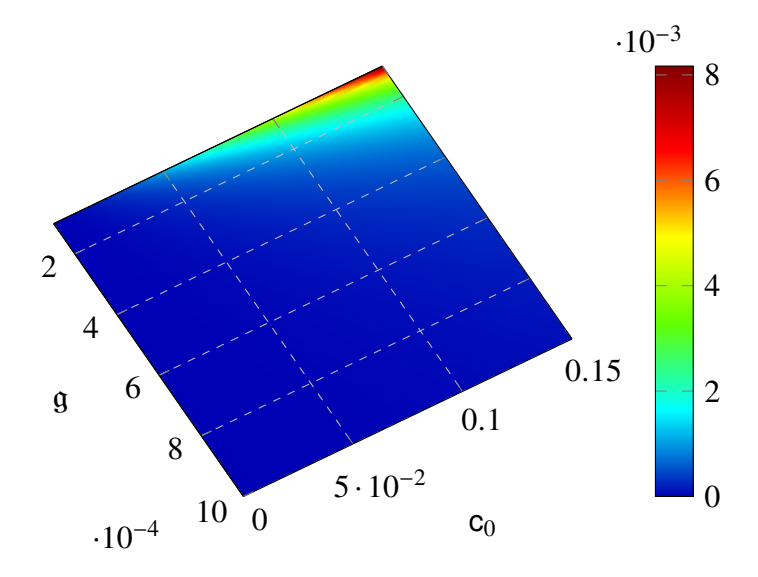


Fig. 7. Level curves threshold \mathcal{T} as a function of \mathfrak{g} and c_0 , with $\mathfrak{g} \in [10^{-4}, 10^{-3}]$ and $c_0 \in [0, 0.15]$.

- Halocline: water density ρ_1 , $\mathfrak{T} = 0^{\circ}$ C, $\mathfrak{S} = 34.2$ psu;
- Atlantic Water: water density ρ_2 , $\mathfrak{T} = 2^{\circ}$ C, $\mathfrak{S} = 34.9$ psu;

and density variations are computed by (see (Talley et al. 2011))

$$\frac{d\rho}{\rho} = -\alpha \, d\mathfrak{T} + \beta \, d\mathfrak{S},\tag{109}$$

where $\mathfrak T$ is the potential temperature, $\mathfrak S$ is the salinity, $\alpha \approx 53 \cdot 10^{-6} \, \mathrm{K}^{-1}$ is the thermal expansion coefficient and $\beta \approx 785 \cdot 10^{-6} \, \mathrm{kg} \, \mathrm{g}^{-1}$ is the haline contraction coefficient. Both α and β depend of the water properties, therefore the value reported here refer only for the Arctic Ocean (see Talley et al. (2011)).

With the above values, the following estimate is obtained for the reduced gravity in (33):

$$g = \left(\frac{\rho_1 - \rho_0}{\rho_0}\right) \frac{\rho_2}{\rho_1} g \approx 8 \cdot 10^{-4} \,\text{ms}^{-2},\tag{110}$$

and, as $f = 2\Omega \approx 1.5 \cdot 10^{-4} \, \text{s}^{-1}$ and assuming $c_0 \approx 0.1 \, \text{ms}^{-1}$ we have the following estimate for the right-hand side of (108)

$$\mathcal{F}(\mathfrak{g}, \mathbf{c}_0) = \frac{f^2 \mathbf{c}_0^2}{(\mathfrak{g}^2 + f^2 \mathbf{c}_0^2)} \frac{(f^2 \mathbf{c}_0^2 - \mathfrak{g}^2)^2}{\left[5f^4 \mathbf{c}_0^4 + 5\mathfrak{g}^4 + 6f^2 \mathbf{c}_0^2 \mathfrak{g}^2\right]} \approx 0.00007. \tag{111}$$

It decreases as the amplitude of c_0 decreases, while it increases as \mathfrak{g} decreases. See Fig. 7.

As an example, its value is about 0.000045 if $|c_0| \approx 0.01 \, \text{ms}^{-1}$, implying that as the intensity of the mean current above that halocline c_0 decreases, the nonlinear flow in more prone to become unstable.

It is also worth giving some numerical estimates of the left-hand side of (108), namely, the steepness of the wave, because, even if the threshold \mathcal{T} is small (see Figure 6, Figure 7 and (111)), the instability may not always occur, as also the steepness of the wave could be a very small.

From (10) and (35), we can write

$$m^{2} = \frac{g^{2}k^{4}c^{2}}{f^{4}c_{0}^{2}} = \frac{g^{2}k^{2}}{f^{2}c_{0}^{2}} \left(1 + \frac{f^{2}c_{0}^{2}}{g^{2}}\right) \approx \frac{g^{2}k^{2}}{f^{2}c_{0}^{2}},$$
(112)

and, fixing $g := \left(\frac{\rho_1 - \rho_0}{\rho_0}\right) \frac{\rho_2}{\rho_1} g \approx 8 \cdot 10^{-4} \, \text{ms}^{-2}$, $f = 2\Omega \approx 1.5 \cdot 10^{-4} \, \text{s}^{-1}$ and $c_0 \approx -0.1 \, \text{ms}^{-1}$ we have the following values of m as a function of k:

$$m \approx \frac{\mathfrak{g}}{f|\mathbf{c}_0|} k \approx \begin{cases} 0.08 \,\mathrm{m}^{-1} & \text{for } k = 0.0015 \,\mathrm{m}^{-1} & \text{i.e. } L \approx 4.2 \,\mathrm{km}, \\ 0.33 \,\mathrm{m}^{-1} & \text{for } k = \frac{\pi}{500} \,\mathrm{m}^{-1} & \text{i.e. } L = 1 \,\mathrm{km}, \\ 1 \,\mathrm{m}^{-1} & \text{for } k = \frac{3}{160} \,\mathrm{m}^{-1} & \text{i.e. } L \approx 335 \,\mathrm{m}. \end{cases}$$
(113)

Fixing a = 10, and recalling that $d_0 - s_-(r)$ is the mean depth of the halocline base at a fixer r and that $s \ge s_-(r)$, if s = 1 and k = 0.0015 we have that $e^{-2ms} \approx 0.85$ and instability occur, while if s = 15 $e^{-2ms} \approx 0.09$ and instability may or may not occur.

In fact, the inequality (108) is just sufficient condition for instability to emerge, but there could be other ξ and \mathbf{A} for which the threshold \mathcal{T} is even small, and so even the condition a = 10, k = 0.0015 and s = 15 may be unstable.

In general, it can be said that the occurrence or not of the instability is related with the length of the waves and their depth, with deeper (hence taller waves, see (8) and (16), and the discussion in Puntini (2025a)) and longer being more favorable to be unstable, while shorter and less deep waves are less prone to become unstable.

Acknowledgments. The author is supported by the Austrian Science Fund (FWF) [grant number Z 387-N].

The author declare no conflicts of interest.

Data availability statement. No data were created or used for this paper.

References

- Abrashkin, A. A., and E. N. Pelinovsky, 2022: Gerstner waves and their generalizations in hydrodynamics and geophysics. *Phys.-Uspekhi*, **65** (**5**), 453–467, https://doi.org/10.3367/UFNe.2021. 05.038980.
- Bayly, B. J., 1987: *Three-dimensional instabilities in quasi-two dimensional inviscid flows*, 71–77. American Society of Mechanical Engineers, New York.
- Bennett, A. F., 2006: Lagrangian Fluid Dynamics. Cambridge University Press, Cambridge.
- Cheng, H., and K. C. Gupta, 1989: An Historical Note on Finite Rotations. *J. Appl. Mech.*, **56** (1), 139–145, https://doi.org/10.1115/1.3176034.
- Chu, J., D. Ionescu-Kruse, and Y. Yang, 2019a: Exact solution and instability for geophysical waves at arbitrary latitude. *Discrete Contin. Dyn. Syst.*, **39** (8), 4399–4414, https://doi.org/10.3934/dcds.2019178.
- Chu, J., D. Ionescu-Kruse, and Y. Yang, 2019b: Exact Solution and Instability for Geophysical Waves with Centripetal Forces and at Arbitrary Latitude. *J. Math. Fluid Mech.*, **21**, https://doi.org/10.1007/s00021-019-0423-8.
- Constantin, A., 2001: Edge waves along a sloping beach. *J. Phys. A: Math. Gen.*, **34**, 9723–9731, https://doi.org/10.1088/0305-4470/34/45/311.
- Constantin, A., 2011: *Nonlinear Water Waves with Applications to Wave-Current Interactions and Tsunamis*, CBMS-NSF Regional Conference Series in Applied Mathematics, Vol. 81. SIAM, Philadelphia.
- Constantin, A., 2012a: An exact solution for equatorially trapped waves. *J. Geophys. Res.*, **117**, C05 029, https://doi.org/10.1029/2012JC007879.
- Constantin, A., 2012b: On the modelling of equatorial waves. *Geophys. Res. Lett.*, **39**, L05 602, https://doi.org/10.1029/2012GL051169.

- Constantin, A., 2013: Some Three-Dimensional Nonlinear Equatorial Flows. *J. Phys. Oceanogr.*, **43**, 165–175, https://doi.org/10.1175/JPO-D-12-062.1.
- Constantin, A., 2014: Some Nonlinear, Equatorially Trapped, Nonhydrostatic Internal Geophysical Waves. *J. Phys. Oceanogr.*, **44**, 781–789, https://doi.org/10.1175/JPO-D-13-0174.1.
- Constantin, A., and P. Germain, 2013: Instability of some equatorially trapped waves. *J. Geophys. Res. Oceans*, **118**, 2802–2810, https://doi.org/10.1002/jgrc.20219.
- Constantin, A., and R. S. Johnson, 2019: *On the role of nonlinearity in geostrophic ocean flows on a sphere*, Vol. 1, chap. D2, 500–519. CRC Press Taylor & Francis Group, Boca Raton.
- Constantin, A., and R. S. Johnson, 2023: On the dynamics of the near-surface currents in the Arctic Ocean. *Nonlinear Anal., Real World Appl.*, **73**, 103 894, https://doi.org/10.1016/j.nonrwa.2023. 103894.
- Constantin, A., and S. G. Monismith, 2017: Gerstner waves in the presence of mean currents and rotation. *J. Fluid Mech.*, **820**, 511–528, https://doi.org/10.1017/jfm.2017.223.
- Drazin, P. G., and W. H. Reid, 2004: *Hydrodynamic Stability*. Cambridge University Press.
- Dubreil-Jacotin, M.-L., 1932: Sur les ondes de type permanent dans les liquides hétérogènes. *Atti Accad. Naz. Lincei, Mem. Cl. Sci. Fis., Mat. Nat.*, **15**, 814–819.
- Friedlander, S., and M. M. Vishik, 1991: Instability Criteria for the Flow of an Inviscid Incompressible Fluid. *Phys. Rev. Lett.*, **66**, 2204–2206, https://doi.org/10.1103/PhysRevLett.66.2204.
- Friedlander, S., and V. Yudovich, 1999: Instabilities in fluid motion. *Not. Am. Math. Soc.*, **46**, 1358–1367.
- Froude, W., 1862: On the rolling of ships. *Trans. Inst. Naval Arch.*, **3**, 45–62.
- Gerstner, F., 1809: Theorie der Wellen samt einer daraus abgeleiteten Theorie der Deichprofile. *Ann. Phys.*, **2**, 412–445.
- Gill, A. E., 1982: Atmosphere-Ocean Dynamics. Academic Press, London.
- Guthrie, J. D., J. H. Morison, and I. Fer, 2013: Revisiting internal waves and mixing in the Arctic Ocean. *J. Geophys. Res. Oceans*, **118**, 3966–3977, https://doi.org/10.1002/jgrc.20294.

- Henry, D., 2008: On Gerstner's Water Wave. *J. Nonlinear Math. Phys.*, **15** (**Suppl 2**), 87–95, https://doi.org/10.2991/jnmp.2008.15.s2.7.
- Henry, D., 2016: Exact equatorial water waves in the f-plane. *Nonlinear Anal. Real World Appl.*, **28**, 284–289, https://doi.org/10.1016/j.nonrwa.2015.10.003.
- Henry, D., and H.-C. Hsu, 2015: Instability of equatorial water waves in the f-plane. *Discrete Contin. Dyn. Syst.*, **35** (3), 909–916, https://doi.org/10.3934/dcds.2015.35.909.
- Ionescu-Kruse, D., 2015a: An exact solution for geophysical edge waves in the f-plane approximation. *Nonlinear Anal. Real World Appl.*, **24**, 190–195, https://doi.org/10.1016/j.nonrwa.2015.02.002.
- Ionescu-Kruse, D., 2015b: On Pollard's wave solution at the Equator. *J. Nonlinear Math. Phys.*, **22**, 523–530, https://doi.org/10.1080/14029251.2015.1113050.
- Ionescu-Kruse, D., 2015c: Short-wavelength instabilities of edge waves in stratified water. *Discrete Contin. Dyn. Syst.*, **35** (5), 2053–2066, https://doi.org/10.3934/dcds.2015.35.2053.
- Ionescu-Kruse, D., 2016a: Instability of equatorially trapped waves in stratified water. *Ann. Mat. Pura Appl.*, **195**, 585–599, https://doi.org/10.1007/s10231-015-0479-x.
- Ionescu-Kruse, D., 2016b: Instability of Pollard's exact solution for geophysical ocean flows. *Phys. Fluids*, **28** (**8**), 086 601, https://doi.org/10.1063/1.4959289.
- Ionescu-Kruse, D., 2017: On the short-wavelength stabilities for some geophysical flows. *Phil. Trans. R. Soc. A*, **376**, 20170 090, https://doi.org/10.1098/rsta.2017.0090.
- Kluczek, M., 2018: Physical flow properties for Pollard-like internal water waves. *J. Math. Phys.*, **19**, 123 102, https://doi.org/10.1063/1.5038657.
- Kluczek, M., and R. Stuhlmeier, 2020: Mass transport for Pollard waves. *Appl. Anal.*, **101** (3), 984–993, https://doi.org/10.1080/00036811.2020.1766029.
- Lifschitz, A., and E. Hameiri, 1991: Local stability conditions in fluid dynamics. *Phys. Fluids*, **3**, 2644–2651, https://doi.org/10.1063/1.858153.
- Longuet-Higgins, M. S., 1969: On the transport of mass by time-varying ocean currents. *Deep Sea Res.*, **16**, 431–447, https://doi.org/10.1016/0011-7471(69)90031-X.

- Maslowe, S. A., 1986: Critical layers in shera flows. *Annu. Rev. Fluid Mech.*, **18**, 405–432, https://doi.org/10.1146/annurev.fl.18.010186.002201.
- McCarney, J., 2023: Exact internal waves in the presence of mean currents and rotation. *J. Math. Phys.*, **64**, 073 101, https://doi.org/10.1063/5.0155193.
- McCarney, J., 2024: Nonhydrostatic internal waves in the presence of mean currents and rotation. *J. Math. Phys.*, **65**, 043 101, https://doi.org/10.1063/5.0176160.
- Metzner, E. P., and M. Salzmann, 2023: Technical note: Determining Arctic Ocean halocline and cold halostad depths based on vertical stability. *Ocean Sci.*, **19**, 1453–1464, https://doi.org/10.5194/os-19-1453-2023.
- Miao, F., M. Fečkan, and J. Wang, 2022: Exact solution and instability for geophysical edge waves. *Comm. Pure Appl. Anal.*, **21** (**7**), 2447–2461, https://doi.org/10.3934/cpaa.2022067.
- Mollo-Christensen, E., 1979: Edge Waves in a Rotating Stratified Fluid, an Exact Solution. *J. Phys. Oceanogr.*, **9**, 226–229, https://doi.org/10.1175/1520-0485(1979)009\(0226:EWIARS\) 2. 0.CO; 2.
- Morison, J., and Coauthors, 2018: The North Pole Region as an Indicator of the Changing Arctic Ocean: The Need for Sustaining Observations. *Arctic*, **71** (**Supplement 1: Arctic Observing Summit 2016**), 1–5, https://doi.org/10.14430/arctic4601.
- Peralta-Ferriz, C., and R. A. Woodgate, 2015: Seasonal and interannual variability of pan-arctic surface mixed layer properties from 1979 to 2012 from hydrographic data, and the dominance of stratification for multiyear mixed layer depth shoaling. *Prog. Oceanogr.*, **134**, 19–53, https://doi.org/10.1016/j.pocean.2014.12.005.
- Pollard, R. T., 1970: Surface waves with rotation: An exact solution. *J. Geophys. Res.*, **75** (**30**), 5895–5898, https://doi.org/10.1029/JC075i030p05895.
- Polyakov, I. V., A. V. Pnyushkov, and E. C. Carmack, 2018: Stability of the arctic halocline: a new indicator of arctic climate change. *Environ. Res. Lett.*, **13**, 125 008, https://doi.org/10.1088/1748-9326/aaec1e.

- Puntini, C., 2025a: Near-inertial Pollard Waves Modeling the Arctic Halocline. *preprint* arXiv:2504.07129.
- Puntini, C., 2025b: On the modeling of nonlinear wind-induced ice-drift ocean currents at the North Pole. *preprint arXiv:2503.12906*.
- Rankine, W. J. M., 1863: On the exact form of waves near the surface of deep water. *Phil. Trans. R. Soc. London A*, **153**, 127–138.
- Reech, F., 1869: Sur la théorie des ondes liquides périodiques. C. R. Acad. Sci. Paris, **68**, 1099–1101.
- Rudels, B., and E. Carmack, 2022: Arctic Ocean Water Mass Structure and Circulation. *Oceanog-raphy*, **35**, 52–65, https://doi.org/10.5670/oceanog.2022.116.
- Stuhlmeier, R., 2013: Internal Gerstner waves: applications to dead water. *Appl. Anal.*, **93** (7), 1451–1457, https://doi.org/10.1080/00036811.2013.833609.
- Stuhlmeier, R., 2014: Internal Gerstner waves on a sloping bed. *Discrete Contin. Dyn. Syst.*, **34 (8)**, 3183–3192, https://doi.org/10.3934/dcds.2014.34.3183.
- Stuhlmeier, R., 2015: On Gerstner's water wave and mass transport. *J. Math. Fluid. Mech.*, **17**, 761–767, https://doi.org/10.1007/s00021-015-0219-4.
- Talley, L. D., G. L. Pickard, W. J. Emery, and J. H. Swift, 2011: *Descriptive Physical Oceanography: An Introduction*. Elsevier, Amsterdam.
- Weber, J. E. H., 2012: A note on trapped Gerstner waves. *J. Geophys. Res.*, **117**, C03 048, https://doi.org/10.1029/2011JC007776.